Journal of Human Evolution 203 (2025) 103674

Contents lists available at ScienceDirect

Journal of Human Evolution

journal homepage: www.elsevier.com/locate/jhevol

Serial reconstruction of Hominini manual phalanges

Miguel López-Cano [a, b, *], Markus Bastir [a]

[a] Paleoanthropology Group, Department of Paleobiology, Museo Nacional de Ciencias Naturales, Calle José Gutiérrez Abascal, 2, 28006, Madrid, Spain
[b] Physical Anthropology Unit, Department of Biodiversity, Ecology, and Evolution, Faculty of Biological Sciences, Universidad Complutense de Madrid, Calle José Antonio Novais, 12, 28040, Madrid, Spain

ARTICLE INFO

Article history:
Received 19 March 2024
Accepted 7 March 2025
Available online 22 April 2025

Handling Editor: Dr S Xing

Keywords:
Hand
Serial homology
Geometric morphometrics
Missing data estimation
Hominins
Panins

ABSTRACT

Serial morphology is the study of repeating, sequentially arranged structures in organisms, focusing on their development, organization, and evolutionary significance. Manual digits in primates, exhibiting proximodistal and radioulnar homology, can be analyzed using a serial morphological approach. This method offers a potential tool for reconstructing serial elements of hominin fossil record. Therefore, this study aims to analyze serial homology in proximal and intermediate phalanges of extant and extinct Hominini species to validate a novel methodology for reconstructing missing bones within the hand. For this purpose, we designed a template (27 true landmarks and 128 curve semilandmarks) for proximal and intermediate phalanges of digits II–V, applied to *Homo sapiens* ($n = 125$), *Homo neanderthalensis* ($n = 9$), *Homo naledi* ($n = 9$), *Australopithecus sediba* ($n = 2$), and *Pan troglodytes* ($n = 122$). Missing data were estimated using bilateral symmetry or geometric estimation methods. We used principal component analysis to quantify and examine morphological variability for each phalanx. Each serially reconstructed phalanx was validated by comparing the estimated to the original morphology using generalized Procrustes analysis and Procrustes distances, principal component analysis, and the Mann-Whitney *U* test. The results highlight both similarities and differences in serial homology between *Pan* and hominins, reflecting a shared developmental 'blueprint' alongside interspecific morphological variations influenced by genetic and functional factors. Finally, serial reconstruction with homologous elements is possible in the proximal and intermediate manual phalanges of Hominini, being more accurate with a proximal-proximal or intermediate-intermediate disposition, offering potential for reconstructing missing fossil hominin manual phalanges.

1. Introduction

When studying hand evolution within the hominin clade, the only available paleontological evidence is derived from hard tissues preserved in the fossil record (Marzke, 1997; Susman, 1998; Tocheri et al., 2008; Trinkaus, 2016; Kivell et al., 2022). However, the scarcity, uneven distribution, and temporal and spatial biases of fossil evidence from the Early and Middle Pleistocene create significant gaps in our understanding of the evolution of hand morphology during these periods. Moreover, the challenge of studying the hominin hand is heightened by its complex structure: it consists of 27 articulated bones, which are mostly found isolated rather than in anatomical connection, making it difficult to assign individual bones to specific species.

Since missing data from broken or unpreserved elements are a common issue in the hominin fossil record, three main methods have been developed to address these limitations. The first method uses information from the same preserved skeletal element (i.e., mirror imaging; Mardia et al., 2000), the second applies geometric techniques to deform and smooth shapes by mapping landmarks and semilandmarks from a reference to a target specimen (i.e., thin-plate spline reconstruction; Gunz et al., 2009), and the third exploits statistical approaches to predict the location of every missing coordinate using multiple regressions based on a sample of complete specimens (i.e., two-block partial least squares; Bookstein et al., 2003). There is also a fourth approach that can integrate all three of the previously mentioned methods as it uses morphological series of homologous elements (e.g., the thoracic spine; García-Martínez et al., 2018). This last method has already proven particularly useful for reconstructing structures from incomplete fossil remains (Bastir et al., 2020).

* Corresponding author.
E-mail address: miguel.lopez@mncn.csic.es (M. López-Cano).

https://doi.org/10.1016/j.jhevol.2025.103674

Serial homology occurs when a structure's underlying genetic program is duplicated, either partially or fully, and expressed at a new time or place during development (Hall, 1995). By definition, serially homologous structures share much of their genetic architecture and developmental processes, establishing basic common body plans or morphologies (Hall, 1992). This principle is evident in the hominin hand, an idea used by Hamrick (2012), who grouped the hand elements into three main modular developmental units (see Fig. 1): a preaxial unit (thumb metacarpus and the first proximal phalanx), a postaxial unit (metacarpals and proximal [PP] and intermediate [IP] phalanges of digits II–V), and a distal phalanx unit. Developmentally, these units form from the lateral plate mesoderm under the influence of gradual expression of *Sonic Hedgehog*, *Hox*, and clock genes each undergoing a distinct morphogenetic process. Specifically, the PP and IP of the postaxial unit are among the first to form in sequence and share unique developmental traits, such as the timing and regulation of *Hoxd11* expression (Reno et al., 2008; Hamrick, 2012).

Furthermore, the postaxial unit is also the most morphologically homogeneous, with PPs and IPs exhibiting the greatest similarity (Patel and Maiolino, 2016; Kavanagh, 2020). Both phalanges share a radioulnarly broad shaft extending distally, trochlea-shaped heads with asymmetrical radial and ulnar halves and radial and ulnar lateral pits. However, they differ in features such as the proximal articular surface—single and vertically oriented in PPs vs. two elliptical facets in IPs—the palmar curvature, and the presence of a median keel.

Given their shared genetic and developmental foundation, the PPs and IPs of the postaxial unit are expected to exhibit a significant morphological covariation (Reno et al., 2008). This relationship can be particularly useful for reconstructing missing phalanges in fossil hominin hands. In the last 15 years, discoveries of partial hand skeletons from *Australopithecus sediba* (Berger et al., 2010) and *Homo naledi* (Berger et al., 2015) have provided relatively complete, semiarticulated, and publicly accessible (https://www.morphosource.org/, Duke University) hand remains from single individuals. The adult *A. sediba* individual 'MH2' preserves a nearly complete right hand skeleton, missing only the distal phalanges of rays 2–5 and three carpal bones (Kivell et al., 2011, 2018). Similarly, the *H. naledi* specimen 'Hand 1' includes all the hand and wrist bones except for the pisiform (Kivell et al., 2015). These well-preserved hands provide a unique opportunity to robustly test the reconstruction of serial homologous phalanges within the hominin fossil record.

Among the features that distinguish the human hand from those of other apes, intrinsic hand proportions are key adaptations for enhanced dexterity and forceful pad-to-pad precision grips (Marzke, 1997; Alba et al., 2003; Feix et al., 2015; Kivell, 2015). Accurately quantifying these proportions requires multiple associated elements from the same individual. Consequently, reconstructing the postaxial unit not only addresses anatomical gaps in fossil specimens but may also provide critical insights into the evolution of manual capabilities and dexterity across hominin lineages.

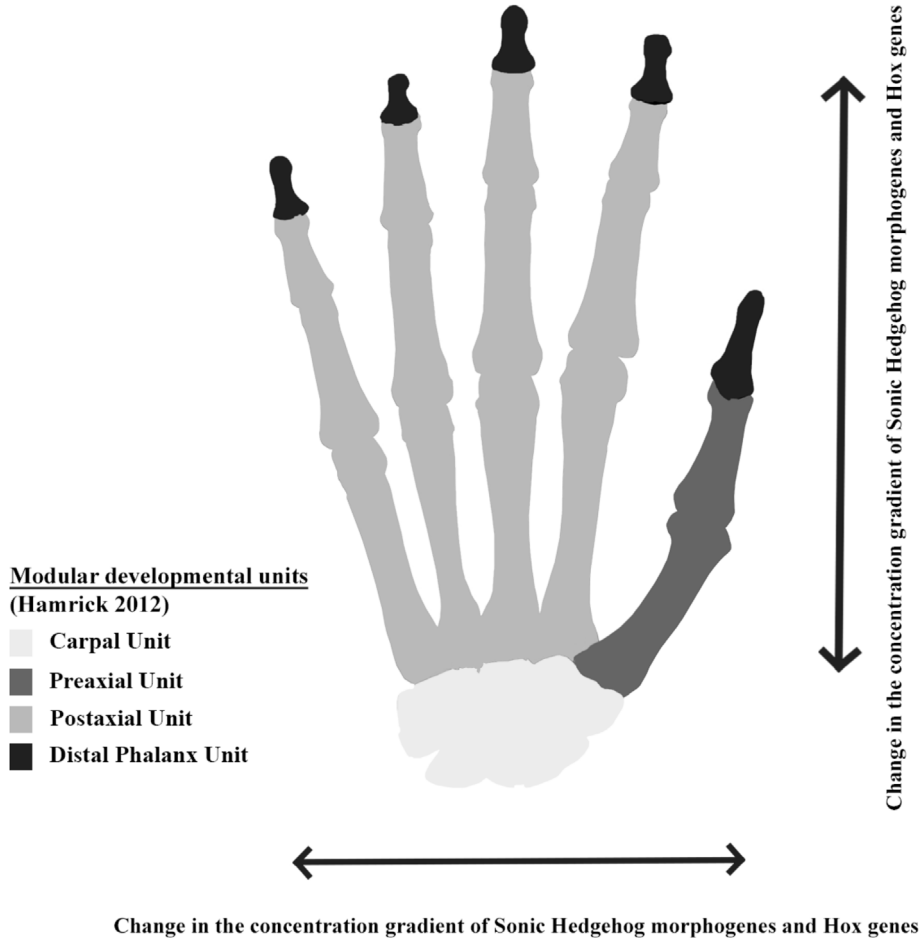

Figure 1. Theoretical modular development units of the hand (Hamrick, 2012). The arrows in both directions indicate gene expression that regulates osteological development.

The principle of serial homology and the modular structure of the hand provide a framework for predicting the morphology of missing elements. We expect that the shape of a PP or an IP can predict the shape of another PP or IP within and between digits in the postaxial unit, using data from a sample of associated individuals (E1). To test E1, we will analyze morphometric data from associated modern and fossil specimens to evaluate whether the preserved elements can accurately predict the morphology of missing counterparts. Support for this expectation would indicate a strong morphological covariation between PPs and IPs, validating the use of serial homology in reconstructions. Conversely, if prediction accuracy is low, it would suggest that other factors (e.g., independent variation or environmental influences) may play a larger role in shaping phalangeal morphology.

Empirical studies suggest that PP and IP of a single digit are highly internally coordinated developmental modules that interact less consistently with the rest of the modules (Klingenberg, 2008; Kavanagh et al., 2013). This morphogenetic and developmental perspective indicates that serial homologs are better defined as structures across rays (e.g., PP to PP) rather than phalanges within the same digit ray (e.g., PP to IP). However, phalanges are also considered "homologous adjacent structures in series" (Kavanagh, 2020: p. 202) with significant morphological similarities. This dual approach—emphasizing developmental modularity within a digit ray and quantifiable morphological similarities across rays—raises questions about the extent to which positional homology (PP to PP or IP to IP) enhances our ability to predict or reconstruct missing elements compared to within-digit serial homology (PP to IP).

Given the stronger morphological and developmental similarity between phalanges occupying the same positional role across digits, we expect them to show greater predictive accuracy and morphological similarity than homologous phalanges across a ray (E2). Quantifying this relationship using three-dimensional geometric morphometric (3DGM) techniques would allow for a direct test of whether positional homology provides a more robust basis for reconstructing missing phalanges than serial proximodistal homology. Greater predictive power from positional homologs would support the expected, while comparable or superior predictive power from serial proximodistal homologs would falsify it, indicating that shared genetic and developmental pathways within a ray play a larger role in shaping phalangeal morphology.

The examination of serial homology within the phalanges not only provides insights into reconstructing missing elements but also offers a foundation for exploring broader evolutionary questions. Panins and modern humans' digits, as closest living relatives (Mikkelsen et al., 2005), share a common genetic and developmental 'blueprint,' which constrains their capacity to vary independently (Rolian et al., 2010). This genetic limit leads to similar patterns of phenotypic variation in both size and shape across these species, despite their differing morphology (e.g., phalangeal curvature angle or body length), lifestyles, and functional demands (e.g., knuckle-walking vs. bipedalism). Nevertheless, it is unclear to what extent this species-specific adaptation restricts their serial homology of PPs and IPs.

To investigate this, it is important to quantify and compare the serial deformation of PPs and IPs in both species. Serial deformation refers to the measurable changes in shape and geometry that occur between homologous skeletal elements within a series, such as the PPs and IPs of the hand (Kavanagh, 2020). We expect that the deformation patterns of serial homologs (PPs and IPs) differ between hominins and *Pan troglodytes* due to their distinct morphology, manual adaptations, and functional constraints (E3). We will use 3DGM analyses to quantify and compare serial deformation patterns of PPs and IPs between Hominini species. Significant differences in deformation patterns would indicate the influence of species-specific functional or genetic causes. Conversely, a lack of significant differences would suggest that shared genetic constraints play a dominant role in shaping these patterns, over-riding functional divergence.

2. Materials and methods

2.1. Sample and scanning techniques

The sample consisted of 3D models of II–V PPs and IPs of *Homo sapiens* (*Hs*), *Pan troglodytes* (*Pt*), *Homo naledi* (*Hn*), *Homo neanderthalensis* (Neanderthals), and *Australopithecus sediba* (*As*) (see Fig. 2).

The 3D models were gathered from the collections of the National Museum of Natural Sciences (MNCN, Madrid), the National Museum of Natural History (Paris), and online repositories including Morphosource (www.MorphoSource.org, Duke University) and The Human Fossil Record (www.human-fossil-record.org). Clinical CT data were acquired at the National Centre for Accelerators (Seville) through collaboration between the MNCN and Charles University, independent of this study. The dataset obtained via clinical CT scans received ethical approval from the Faculty of Sciences, Institutional Review Board of Charles University (2024/03), and a written informed consent was obtained from the participants, adhering to the Helsinki Protocol (Goodyear et al., 2007), ensuring anonymization of the data.

The modern human sample included 17 healthy adults (11 males and six females, aged 59–74 years) housed at the MNCN. Additionally, we incorporated a 28-year-old female climber with over six years of experience in free climbing, who trains four times per week, scanned at the National Centre for Accelerators, and two archaic *Hs* individuals (Arene Candide 2 and Nazlet Khater 2) housed at the Archaeological Museum of Finale and the National Museum of Egyptian Civilization, respectively. The *Pt* sample consisted of 12 wild-shot healthy adults (five males, four females, and three of undetermined sex), obtained from the National Museum of Natural History.

The *Hn* and *As* samples consist of previously published phalanges of specimens 'Hand 1' and 'MH2' (Kivell et al., 2011, 2015), housed at the Evolutionary Studies Institute at the University of the Witwatersrand. These 3D models were downloaded from Morphosource. For 'MH2,' only the fourth and fifth IPs of the right hand were analyzed as the 3D model of the left hand is in anatomical articulation, preventing accurate measurements. The Neanderthal sample comprised hand phalanges of Shanidar 3 and Spy 2, housed at the Smithsonian National Museum of Natural History and the Royal Belgian Institute of Natural Sciences, respectively.

The main sample focuses on *Pt* and *Hs* as they, along with bonobos, are the closest living relatives (Mikkelsen et al., 2005) and with extensive available data on both hand morphology and functional anatomy (Susman, 1979; Marchi, 2005; Lazenby et al., 2011; Wallace and Patel, 2013; Syeda et al., 2023, 2024), providing a robust comparative framework to study serial reconstruction in hominin evolution.

The PPs and IPs of *Hs* and *Pt*, excluding the 'climber' and both archaic *Hs* individuals, were scanned using a high-resolution Artec Space Spider Scanner with a resolution of 0.1 mm and an accuracy of 0.05 points per mm. The resulting 3D meshes were post-processed using Artec Studio v. 16 (3D Systems, Rock Hill). For the 'climber,' a Spiral Acquisition by a Siemens Biograph CT scanner with settings of 120 kV, 160 mAs, and 0.6 mm slice thickness was used. Routine matrix clinical images were reconstructed using the high-resolution B30F kernel for hard tissues assessment. High-resolution μCT scans of Arene Candide 2 PPs and IPs were collected using a SkyScan 1173 at 100–130 kV, 61–62 μA; and the scans

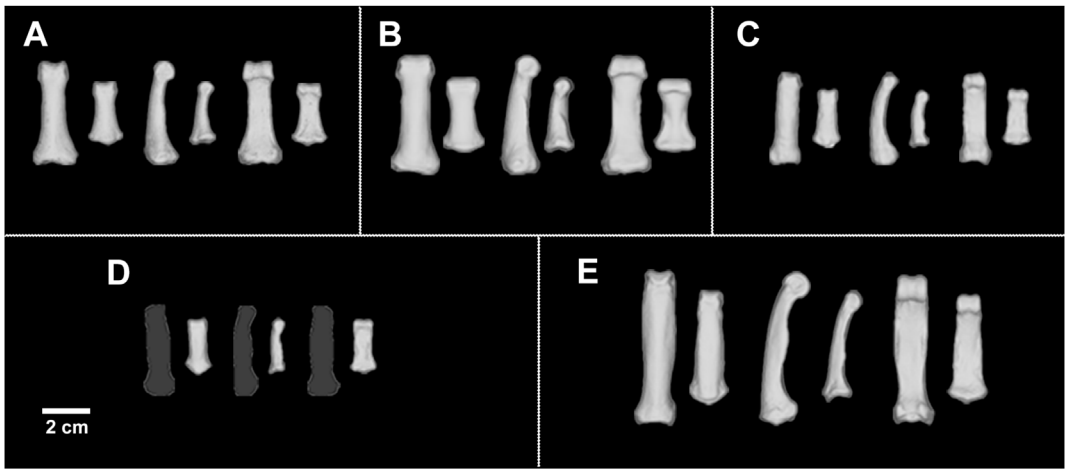

Figure 2. A subset of the sample by species considered in this study in dorsal, lateral, and palmar views (left to right). (A) PP2 and IP2 of Arene Candide 2 (*Hs*); (B) PP3 and IP3 of Shanidar 3 (Neanderthal); (C) PP3 and IP3 of U.W. 101 (*Hn*); (D) PP4 (in dark gray as it was not considered in the study) and IP4 of MH2 (*As*); (E) PP4 and IP4 of MNHN 1901-659 (*Pt*). *As = Australopithecus sediba; Hn = Homo naledi; Hs = Homo sapiens; IP = intermediate phalanx; PP = proximal phalanx; Pt = Pan troglodytes.*

resolution ranged between 0.030 and 0.042 mm. Nazlet Khater 2 PPs and IPs μCT scans were collected using the GE phoenix v | tome | x L 240–180 at 180–240 kV, 300 μA, and 0.11 mm scan resolution. The 3D models from the CT and μCT scans were generated using Slicer 4.10.2 software (www.slicer.org; Fedorov et al., 2012). Every 3D model was exported as .ply files.

2.2. Landmark measurements and basic three-dimensional geometric morphometric analysis

The shape of each phalanx was quantified by 3DGM using Viewbox 4.0 (Dhal, Kiffisia), following standard processes for analyses and visualizations in virtual morphology and morphometrics (Bastir et al., 2019). Previous studies have demonstrated the comparability of landmarks measurements on 3D models obtained from clinical CT scans, high-resolution μCT scans, and high-quality surface scanners in geometric morphometrics analysis (Ross and Williams, 2008; Brzobohatá et al., 2012; Rosas et al., 2016; Bastir et al., 2017; Shearer et al., 2017; D'Angelo del Campo et al., 2023; for further details, please see Supplementary Online Material [SOM] S3).

Four of the analyzed fossil phalanges had missing data. For both PP2 phalanges of Shanidar and the left PP3 of *Hn*, missing data were estimated using mirror imagining (i.e., mirror imaging; Mardia et al., 2000). For the PP5 of *Hn*, TPS interpolation was applied using PP4 from the same side of 'Hand 1' to estimate the missing coordinates (Gunz et al., 2009).

We developed a template for both PPs and IPs comprising 155 points, consisting of 27 landmarks linked by 128 curve semilandmarks. (For further details please see SOM S1.) The template was designed to exclude anatomical regions related to functionality (e.g., entheses) and instead focuses on regions shared by both PPs and IPs that hold morphological potential for serial reconstruction. The semilandmark data were slid and reslid in the Viewbox 4.0 software to align with the Procrustes sample average, following standard procedures (Gunz et al., 2005; Mitteroecker and Gunz, 2009; Gunz and Mitteroecker, 2013; Bastir et al., 2019). All landmarks and semilandmarks were subjected to a generalized Procrustes analysis (GPA).

2.3. Intraobserver error test

To ascertain the repeatability of the measurements, we conducted an intraobserver error (IOE) test in three distinct phases (see SOM S3 for further details). First, we measured three sets of measurements, spaced one week apart, from three randomly selected individuals of both *Hs* and *Pt* and contrasted the Procrustes distances (PDs) between these individuals and the sample. Second, we calculated the percentage of individuals whose PDs were smaller than that among the IOE replicates. To determine whether the variation was due to a measurement error or actual biological shape variation, we assessed the error at two levels: interspecific (*Hs* and *Pt*) and interdigit. Third and in line with this previous analysis, we remeasured a PP2 and a IP2 from two randomly selected *Hs* over two days and compared their coordinates and vectors with the entire sample of PP2 and IP2 through a principal component analysis (PCA; please see Fig. 3 and SOM S3 for more details) at two different levels: the vector between each phalanx repetition and the vector between the mean shape of each phalanx and its serial counterpart within the entire sample (e.g., PP2 to PP3 or PP2 to IP2).

Intraobserver error was considered acceptable if the largest PD resulting from repeated measurements on the same specimen was smaller than the smallest distance between distinct specimens (Bastir et al., 2014, 2017) or if its signal differed from that produced by true biological shape variation (Engelkes et al., 2019).

2.4. Serial homology analysis

The first step in understanding the potential for serial reconstruction of the phalanges has been to evaluate their differences in shape. To achieve this, after performing a GPA and PCA with the entire sample, we grouped the phalanges with their potential homologs from both the radioulnar axis between digits (e.g., PP2-PP3) and the proximodistal axis within the same digit (e.g., PP2-IP2). Subsequently, we conducted specific GPAs and PCAs (Mitteroecker and Gunz, 2009) and established the vector between the mean shapes for each phalanx and taxon. Additionally, to facilitate morphological interpretation, we warped the individual closest to the extreme positive and negative values of each principle component to the shape coordinates representing those extremes (Bastir et al., 2019).

2.5. Reconstruction using serial homology

To assess the potential of seriality patterns for reconstructing missing phalanges, we conducted an experiment adapted to the

available sample. For *Hs* and *Pt*, where a larger sample is available, we used the mean shape of the phalanges and compared it to a randomly selected 'problem case' to test reconstruction accuracy. We tested the potential for reconstruction based on morphological homology along the ulnoradial axis (e.g., for IP3, we used IP2 and IP4) and the proximodistal axis (e.g., for IP3, we used PP3). First, a GPA was performed to align the 'problem case' phalanx and the mean shapes. Then, the morphological variation observed between the mean shapes was applied to the 'problem case' phalanx to estimate each serially reconstructed phalanx, and the PDs of the reconstructions were compared to the original to evaluate accuracy (Zelditch et al., 2012). Next, we used a Mann-Whitney *U* test with principal component 1 (PC1) scores to compare the selected reconstructed phalanx to the rest of the same digit and species sample. Finally, we performed a PCA to ensure the reconstructed phalanges fell within the original sample's morphological space, including the 95% confidence ellipsoid (please see SOM S4).

For the fossil sample (Neanderthals and *Hn*), we only considered for reconstruction those with more than one phalanx from the same digit and segment, and aimed to serially reconstruct those that also had the original phalanx. We also maintained the test for serial homology in both the radioulnar and proximodistal axes. Once again, the first step was to perform a GPA with the phalanges under study. Next, we calculated the morphological variation in each axis of phalanges from the same individual, which was then applied to another phalanx on that axis within the same species to estimate its serial reconstruction. Additionally, we tested the same process by applying the serial deformation vector from *Hs*. Afterward, all reconstructions were compared to the original using PDs to select the most accurate one. Finally, as a statistical check, we performed another Mann-Whitney *U* test following the same procedure mentioned earlier.

The 3DGM and statistical analyses were performed in R v. 4.3.2 (R Core Team, 2023) using the packages 'Morpho' v. 2.13 (Schlager, 2017), 'Geomorph' v. 4.0.6 (Adams et al., 2023), 'ggplot2' v. 3.5.1 (Wickham, 2016), 'dplyr' v. 1.1.4 (Wickham et al., 2023), 'tidyr' v. 1.3.1 (Wickham et al., 2024), 'stringr' v. 1.5.1 (Wickham, 2023), 'patchwork' v. 1.3.0 (Pedersen, 2024), and 'Rvcg' v. 0.22.2 (Schlager, 2017). Please see SOM S2 for further details.

3. Results

3.1. Intraobserver error

The results of the first and second phases of the IOE test indicate that 99.04% of the analyzed sample meet the criteria for repeatability as their PDs are higher than the highest observed error PD (0.05; please see SOM S3 for further details). This IOE does not occur at interspecific or interdigit levels, meaning that this variation is relatively small compared to the true biological shape variation. Furthermore, as shown in Figure 3, the variation among the IOE repetitions is not comparable to the biological differences in shape among the phalanges. The IOE vectors have a different magnitude, direction, and orientation from those established between the shapes of serial phalanges.

Hence, despite larger absolute levels of IOE in few cases, the fact that all specimens in our superimposed landmark dataset were well separated along the first principal components shows that landmark data acquired by the same observer can give results that are precise enough to allow correct biological inferences (Engelkes et al., 2019). Thus, we believe that there is convincing evidence to argue that the measurement error does not affect the reliability of our study in analyzing the serial reconstruction capability in hominins and *Pt* phalanges.

3.2. Serial reconstruction

The phalanges with the most accurate reconstructions were positionally homologous along the radioulnar axis (PP-PP or IP-IP, Table 1, and for further details, see SOM S4), even though the fossil-reconstructed phalanges following the proximodistal axis were also accurate and statistically reliable.

Only in the cases of PP2 and PP5, we observe a difference between the closest serially reconstructed phalanx of *Hs* and *Pt*. For *Hn*, only PP2, PP4, and IP3 were reconstructed due to limited sample availability, with just two PP3 and IP3 phalanges. In Neanderthals, we used PP2 and IP3 to reconstruct PP3, PP4, and IP4, and IP2 was excluded due to the absence of an original phalanx for comparison.

Importantly, Mann-Whitney *U* tests and PCAs revealed no statistically significant differences between the original and reconstructed phalanges. All reconstructed phalanges of *Hs* and *Pt*, when compared to the rest of the phalanges in the sample from the same segment and digit, fall within the 95% confidence region in PC1 and PC2 (see SOM S4), which validates serial reconstruction of these species in PPs and IPs. However, the high *p* value observed in fossil-reconstructed phalanges likely reflects the small sample size; future studies with larger samples on partially complete hands will be necessary to strengthen these results.

3.3. Seriality in proximal and intermediate phalanges

In the serial morphological analysis of PPs and IPs in Hominini, we found distinct deformation patterns of serial homologous phalanges between *Hs* and *Pt*, with all hominin species clustering within a shared region, clearly separating them from chimpanzees (see Figs. 4 and 5). Across species, the vectors of serially homologous phalanges exhibit similar deformation magnitudes, except for Neanderthals. This exception is likely due to the limited sample size and their particular shape (relatively broad epiphyses) compared to other hominins; future studies with larger samples will be necessary to confirm these anomalous distinctive patterns.

Both in the comparison of serially homologous phalanges along the radioulnar and proximodistal axes (Figs. 4 and 5 respectively), PC1 (explaining 53–74.4% of the total variance) primarily captures the anatomical features that distinguish hominins from panins, such as the phalangeal curvature, the radioulnar extension, and the body shape. However, PC2 (explaining 3.6–9.7% of the total variance) reveals greater variation depending on whether the serial homology involves positionally homologous phalanges or not. In the case of positionally homologous phalanges, they do not show a clear differentiation in the clustering (Fig. 4). Conversely, when comparing PPs and IPs of the same digit, they cluster separately, highlighting their distinct anatomical traits, like their body shape or the proximal articular surface.

Consistent with the previous results, along the radioulnar axis (Fig. 4), interdigital differences are minimal, with smaller vectors between mean shapes. In contrast, the proximodistal axis (Fig. 5) shows greater differentiation and the magnitude of the vectors increases. Thus, positional homologous phalanges display higher morphological similarity, with smaller deformation vectors and clustering closer than proximodistal homologous phalanges.

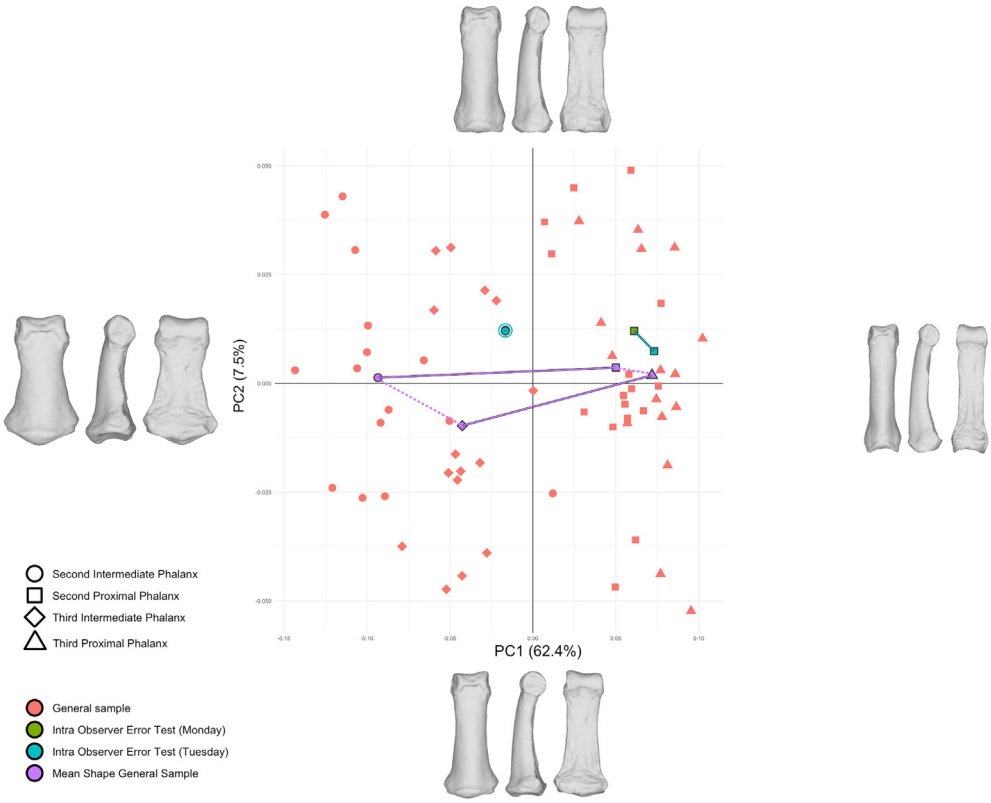

Figure 3. A principal component analysis illustrating the shape variance between PP2-PP3 and IP2-IP3 in the studied sample and the IOE test for PP2 and IP2. Circle: IP2; square: PP2; diamond: IP3; triangle: PP3; red: general sample; green: mean shape from Monday IOE test; blue-green: mean shape from Tuesday IOE test; purple: mean shape of the general sample. IOE = intraobserver error; IP = intermediate phalanx; PC1 = principal component 1; PC2 = principal component 2; PP = proximal phalanx. (For interpretation of the references to color in this figure legend, the reader is referred to the Web version of this article.)

Table 1
Phalanx-based serial reconstruction across species and comparison of reconstruction vs. original using the Mann-Whitney *U* test.

		Homo sapiens (Hs)	*Pan troglodytes (Pt)*	*Homo naledi (Hn)*			*Neanderthals*	
PP2	CSRP	PP4	PP3				PP3[a]	PP4[a]
	PD	0.051	0.044				0.085	0.085
	p	0.823	0.56				1	1
PP3	CSRP	PP4	PP4	PP2[a]	PP4[a]	IP3[a]		
	PD	0.044	0.034	0.065	0.065	0.066		
	p	0.941	0.381	1	1	1		
PP4	CSRP	PP3	PP3					
	PD	0.044	0.035					
	p	0.824	0.45					
PP5	CSRP	PP2	PP4					
	PD	0.057	0.056					
	p	0.588	0.75					
IP2	CSRP	IP3	IP3					
	PD	0.091	0.056					
	P	0.25	0.4					
IP3	CSRP	IP4	IP4				PP3[a]	IP4[a]
	PD	0.061	0.038				0.052	0.053
	p	0.875	0.737				1	1
IP4	CSRP	IP3	IP3					
	PD	0.062	0.038					
	p	0.941	1					
IP5	CSRP	IP2	IP2					
	PD	0.078	0.055					
	p	0.5	0.6					

Abbreviations: CSRP = closest serially reconstructed phalanx; IP = intermediate phalanx; PD = Procrustes distance; PP = proximal phalanx.
[a] The CSRP has been following the fossil deformation vector.

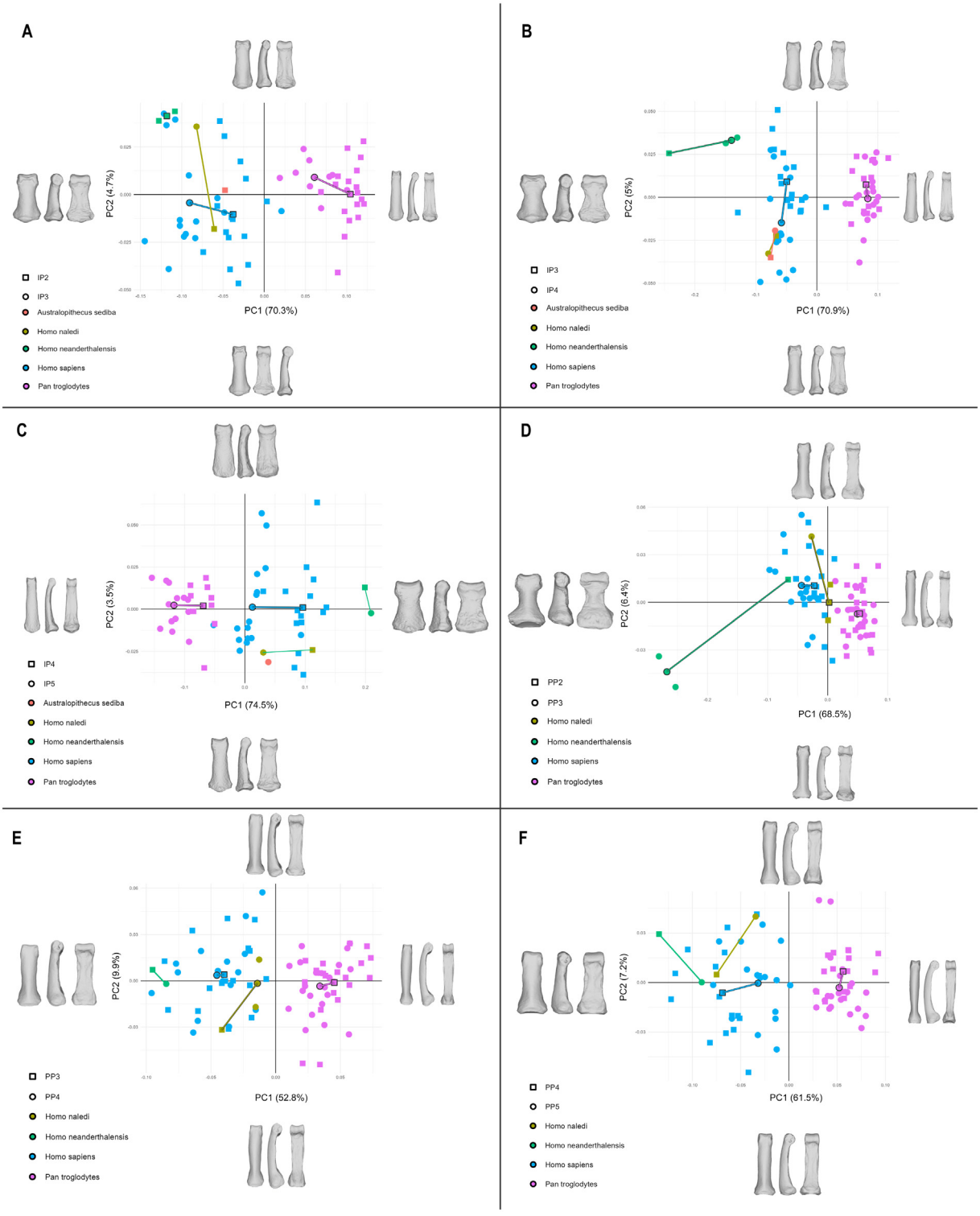

Figure 4. Principal component analyses illustrating the shape variance between phalanges following the radioulnar axis. (A) IP2-IP3; (B) IP3-IP4; (C) IP4-IP5; (D) PP2-PP3; (E) PP3-PP4; (F) PP4-PP5. IP = intermediate phalanx; PP = proximal phalanx. (For interpretation of the references to color in this figure, the reader is referred to the Web version of this article.)

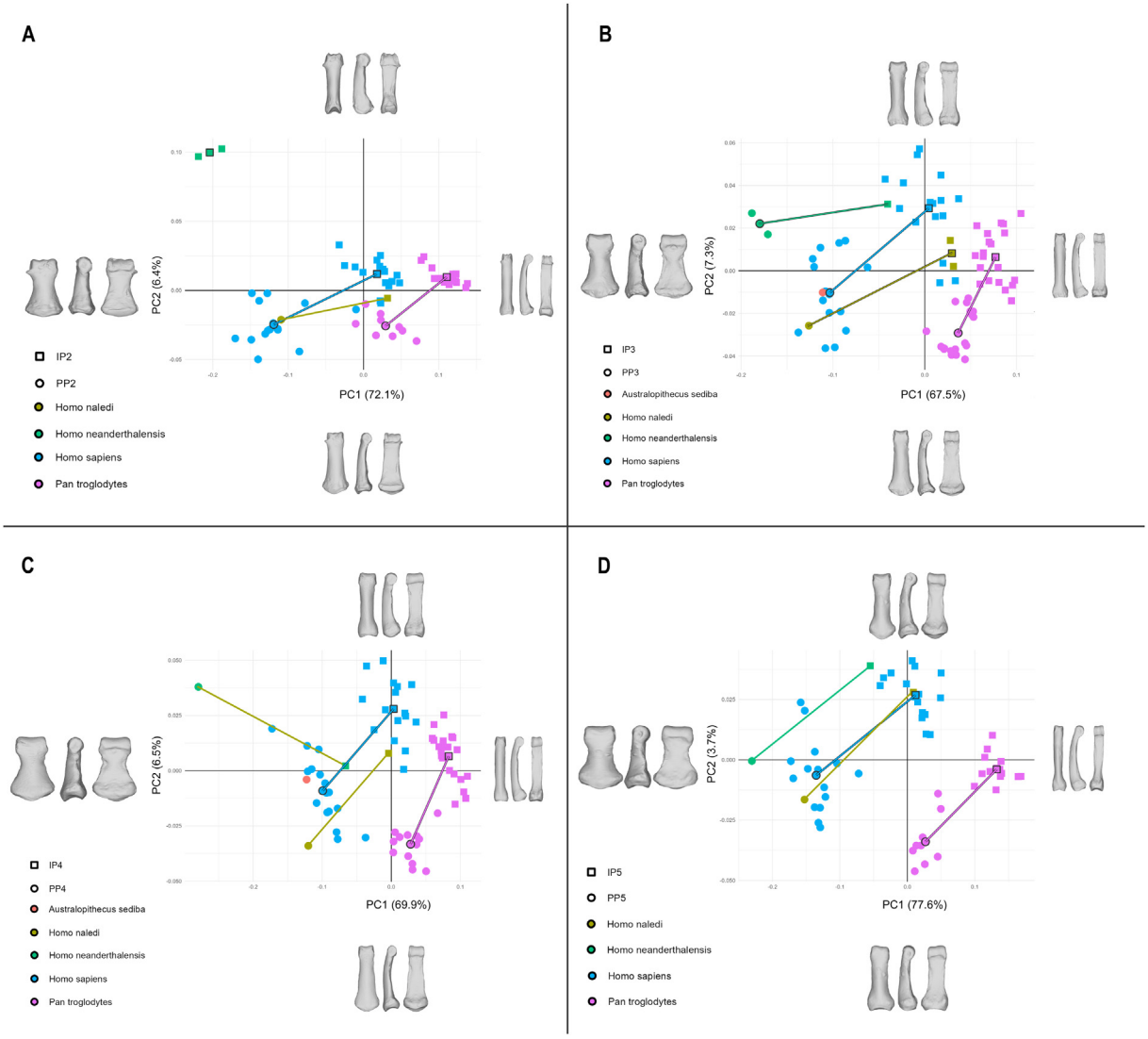

Figure 5. Principal component analyses illustrating the shape variance between phalanges following the proximodistal axis. (A) PP2-IP2; (B) PP3-IP3; (C) PP4-IP4; (D) PP5-IP5. IP = intermediate phalanx; PP = proximal phalanx. (For interpretation of the references to color in this figure, the reader is referred to the Web version of this article.)

4. Discussion

In this study, we explored the morphological seriality and homology between PPs and IPs of the postaxial unit in Hominini to test E1–E3 regarding serial deformation patterns and their potential for reconstructing missing skeletal elements within the hand in fossil specimens.

4.1. Shape covariation of proximal and intermediate phalanges

We expected that the shape of a PP or an IP could predict the shape of another PP or IP within and between manual digits if using the deformation vector and data from E1. Our results confirm a significant morphological covariation between PPs and IPs, which is consistent with theoretical models of metameric development (Hamrick, 2012) but seems to contradict the concept of phalanges as modular structures with independent development (Klingenberg, 2008; Kavanagh et al., 2013). However, Kavanagh (2020) also describes phalanges as "homologous adjacent structures in series" (p. 202), which support the existence of serial homology between the external shape of PPs and IPs. These findings validate E1 and demonstrate the feasibility of using this morphological serial covariation for reconstructing missing phalanges as we have statistically validated.

4.2. Positional vs. proximodistal homologs

Building on the confirmation of PP and IP as serial homologs, we tested whether positional homologs (PP-PP or IP-IP) provide greater predictive accuracy than serial homologs along the proximodistal axis within the same digit (PP-IP). Our findings support E2. As shown in Figures 4 and 5, positional homologs cluster closer than PP-IP, and also the reconstructions based on positional homologs yielded more accurate results for *Hs* and *Pt*. This can be attributed to their higher degree of anatomical similarity and shared developmental modularity (Klingenberg, 2008; Kavanagh et al., 2013), as well as their distinct functional roles in chimpanzees (Matarazzo, 2015; Syeda et al., 2024).

However, we also found that reconstructions based on same-digit proximodistal serial homologous phalanges can produce statistically reliable results, though with reduced accuracy. Therefore, we recommend prioritizing positional homologous phalanges for future reconstructions if possible.

This validated reconstruction approach using serial deformation of homologous bones as PPs and IPs may be particularly useful for other fossil sites where incomplete but associated manual PPs and IPs are preserved, such as L.H. 21 (*Australopithecus afarensis*; White, 1980), DIK-1-1 (*A. afarensis*; Alemseged et al., 2006), OH 7 (*Homo habilis*; Napier, 1962), KNM 47000 (*Paranthropus boisei*; Richmond et al., 2020), and LB1 and LB6 (*Homo floresiensis*; Larson et al., 2009). For Neanderthals and modern humans, examples include Shanidar 4 and 6 (*H. neanderthalensis*; Trinkaus, 1983; Niewoehner, 2006) and El Mirón 1 (*H. sapiens*; Carretero et al., 2015). Applying this method to these individuals could enhance our understanding of the evolution of intrinsic hand proportions and manual dexterity during human evolution.

4.3. Seriality differences between proximal and intermediate phalanges

To explore this covariation between PP and IP in Hominini, we compared the two best studied species, *Hs* and *Pt*. We expected the deformation pattern of serial homologous phalanges to differ due to their distinct morphology, manual adaptations, and anatomical constraints (E3), and our results partially reject E3. On the one hand, similarities in the magnitude and direction of PP-PP, IP-IP, and PP-IP deformation vectors in *Hs* and *Pt* support the idea of a shared genetic and developmental 'blueprint' of both species (Rolian et al., 2010), which is also consistent with theoretical arguments of PP-IP undergoing the same metameric development within primates (Hamrick, 2012). On the other hand, the phalanges of modern humans and chimpanzees occupy distinct spaces in PCAs, reflecting their morphological differences, likely driven by genetic, functional, and behavioral adaptations (Susman, 1979; Inouye, 1991, 1992, 1994; Rasmussen and Tan, 1992; Prabhakar et al., 2008; Patel and Maiolino, 2016).

Focusing on functional traits that are genetically determined and shaped by adaptation, researchers have primarily examined manipulation and locomotion differences between panins and hominins (Susman, 1979, 1998; Marchi, 2005; Matarazzo, 2013; Kunze et al., 2024). *Hs*, Neanderthals, *Hn*, and *As* locomotion is bipedalism, though the latter two exhibit certain arboreal adaptations (Kivell et al., 2011, 2015). In contrast, *Pt* engages in a specialized form of terrestrial quadrupedalism known as knuckle-walking and also displays a greater degree of arboreality than the other hominines (Hunt, 2020; Syeda et al., 2023, 2024). These functional adaptations are reflected in their anatomical features such as the included angle and the flexor sheath ridges (Susman, 1979; Susman et al., 1984).

Among hominins, *Hn* and *As* show serial deformation vectors closer to *Hs*, confirming shared morphological features (e.g., reduced phalangeal flexor sheath ridges, Kivell et al., 2011, 2015). Neanderthals, however, show a completely distinct signal when compared to the other Hominini analyzed. There are several traits on their phalanges which differentiate them from *Hs*, but many researchers have mainly focused on one feature: their relatively broad epiphyses involving both the distal trochlea and the articular facets and lateral tubercles on the bases of PP and IP (Musgrave, 1973; Trinkaus, 1983; Trinkaus et al., 2007; Semal et al., 2009). However, due to the small fossil sample size, further research increasing the analyzed individuals is needed to refine these observations and clarify the serial deformation vectors of PPs and IPs in human evolution.

4.4. Step-by-step protocol for future fossil serial reconstruction

Based on our findings, we propose the following protocol for applying serial reconstruction to fossil phalanges. The first step involves identifying which phalanges, either PP or IP, are missing from the fossil specimen. It is important to mention that to establish a serial deformation vector, it is necessary to have at least two PPs, two IPs, or one of each. If only one phalanx is preserved, the researcher can attempt a taxonomic assignment with statistical validation and then use the serial deformation vector of that species to reconstruct its homologous phalanx.

Next, the researcher should establish a comparative dataset of associated PP-IPs, preferably from individuals of the same species and ontogenetic period, to model phalangeal serial deformation. When both positional homologous phalanges are available, they should be prioritized for reconstruction due to their higher morphological similarity and predictive accuracy. If not, it is also possible to apply the deformation vectors following the proximodistal axis of homologous phalanges within the same digit.

The final step involves validating the reconstructions. This can be achieved through a GPA comparing the PDs, followed by a PCA with 95% confidence ellipsoid.

4.5. Limitations

There are some limitations to our study that should be acknowledged. First, our study is founded upon morphological traits of PPs and IPs resulting from their external shape. As a result, any assumption regarding functional adaptations must be interpreted with caution since this approach does not consider that other factors as genetics, age, hormonal variation, or the internal bone structure do also affect the bone shape and development and thus its serial covariation. Indeed, there are other methods that deeply assess manual functional adaptations in bone tissue, such as cross-sectional geometry (Marchi, 2005), trabecular and cortical bone distribution (Tsegai et al., 2013; Syeda et al., 2023, 2024), and 3D entheseal patterns reflecting muscle coordination (Karakostis et al., 2018).

Second, the fossil sample analyzed to validate the reconstruction method remains limited. This constraint is primarily due to taphonomic factors as the fossil record is biased and associated manual remains are rare. A further limitation is the restricted accessibility of associated hands. To strengthen the validation of this reconstruction approach, future research should test it on additional fossil specimens, such as OH 7 or LB1, among others.

5. Conclusions

Our results provide a detailed analysis of the external serial shape covariation between the PP and IP within the Hominini tribe and demonstrate its utility as a reconstruction method. First, we confirm the significant serial covariation of the PP and IP, validating them as homologous elements. Second, we show that this serial covariation can be successfully applied to reconstruct missing manual homologous elements, with positional homologs offering greater accuracy. Finally, we highlight that while certain patterns of this serial homology are shared between hominins and panins because of their common 'blueprint,' there are also differences that point to the distinct genetic and manual functional adaptations across each species.

Declaration of competing interest

The authors declare no conflict of interest.

Acknowledgments

The Spanish Ministry of Science, Innovation and Universities funds this research by a Plan Nacional project to M.B. (PID2020-

115854GB-100) and a predoctoral fellowship to M.L.C. (FPU21/02087). For access to specimens, we thank the following individuals/institutions: Dr. A. Rosas, Museo Nacional de Ciencias Naturales; Dr. L.R. Berger, University of Witwatersrand; Dr. P. Semal, Royal Belgian Institute of Natural Sciences; Dr. M. Tocheri, Canada Research Chair in Human Origins; Dr. J. Cuisin, Muséum national d'Histoire naturelle and Italian Ministry of Cultural Heritage and Activities (as well as the Museo Archaeologico del Finale and V. Sparacello for collecting data from the specimens of Arene Candide). The bones of Nazlet Khater 2 were μCT-scanned, thanks to the ANR project 'Big Dry' (ANR-14-CE31). We thank the coordinator Pr. François Bon and the partners Dr. Isabelle Crevecoeur, Dr. David Pleurdeau, Dr. Joséphine Lesur, and Dr. Chantal Tribolo for granting us access to the material of Nazlet Khater 2. We also want to thank Elena García Vargas, Ángel Parrado, Enrique Guerrero, and Dr. Vladimir Sládek from Charles University Prague for collaboration during the human CT data collection.

Author contributions

Miguel López-Cano: Writing – review & editing, Writing – original draft, Visualization, Validation, Supervision, Software, Resources, Project administration, Methodology, Investigation, Funding acquisition, Formal analysis, Data curation, Conceptualization. **Markus Bastir:** Writing – review & editing, Supervision, Methodology, Investigation, Conceptualization.

Data statement

Since a portion of the 3D model data is still under investigation or subject to sharing restrictions, the models cannot be made openly available. However, landmark data can be shared upon request from the corresponding author.

Supplementary Online Material

Supplementary Online Material related to this article can be found at https://doi.org/10.1016/j.jhevol.2025.103674.

References

Adams, D., Collyer, M., Kaliontzopoulou, A., Baken, E., 2023. Geomorph: Software for geometric morphometric analyses. R package version 4.0.6. https://cran.r-project.org/package=geomorph.

Alba, D.M., Moyà-Solà, S., Köhler, M., 2003. Morphological affinities of the *Australopithecus afarensis* hand on the basis of manual proportions and relative thumb length. J. Hum. Evol. 44 (2), 225–254. https://doi.org/10.1016/S0047-2484(02)00207-5.

Alemseged, Z., Spoor, F., Kimbel, W.H., Bobe, R., Geraads, D., Reed, D., Wynn, J.G., 2006. A juvenile early hominin skeleton from Dikika, Ethiopia. Nature 443, 296–301. https://doi.org/10.1038/nature05047.

Bastir, M., Higuero, A., Ríos, L., García-Martínez, D., 2014. Three-dimensional analysis of sexual dimorphism in human thoracic vertebrae: Implications for the respiratory system and spine morphology. Am. J. Phys. Anthropol. 155, 513–521. https://doi.org/10.1002/ajpa.22604.

Bastir, M., García-Martínez, D., Ríos, L., Higuero, A., Barash, A., Martelli, S., García-Tabernero, A., Estalrrich, A., Huguet, R., de la Rasilla, M., Rosas, A., 2017. Three-dimensional morphometrics of thoracic vertebrae in Neandertals and the fossil evidence from El Sidrón (Asturias, Northern Spain). J. Hum. Evol. 108, 47–61. https://doi.org/10.1016/j.jhevol.2017.03.008.

Bastir, M., García-Martínez, D., Torres-Tamayo, N., Palancar, C.A., Fernández-Pérez, F.J., Riesco-López, A., Osborne-Márquez, P., Ávila, M., López-Gallo, P., 2019. Workflows in a Virtual Morphology Lab: 3D scanning, measuring, and printing. J. Anthropol. Sci. 97, 1–28. https://doi.org/10.4436/jass.97003.

Bastir, M., García-Martínez, D., Torres-Tamayo, N., Palancar, C.A., Benoît, B., Barash, A., Villa, C., Sanchis-Gimeno, J.A., Riesco-López, A., Nalla, S., Torres-Sánchez, I., García-Río, F., Been, E., Gómez-Olivencia, A., Haeusler, M., Williams, S.A., Spoor, F., 2020. Rib cage anatomy in *Homo erectus* suggests a recent evolutionary origin of modern human body shape. Nat. Ecol. Evol. 4, 1178–1187. https://doi.org/10.1038/s41559-020-1240-4.

Berger, L.R., de Ruiter, D.J., Churchill, S.E., Schmid, P., Carlson, K.J., Dirks, P.H.G., Kiibi, J.M., 2010. *Australopithecus sediba*: A new species of *Homo*-like Australopith from South Africa. Science 328 (5975), 195–204. https://doi.org/10.1126/science.1184944.

Berger, L.R., Hawks, J., de Ruiter, D.J., Churchill, S.E., Schmid, P., Delezene, L.K., Kivell, T.L., Garvin, H.M., Williams, S.A., DeSilva, J.M., Skinner, M.M., Musiba, C.M., Cameron, N., Holliday, T.W., Harcourt-Smith, W., Ackermann, R.R., Bastir, M., Bogin, B., Bolter, D., Brophy, J., Cofran, Z.D., Congdon, K.A., Deane, A.S., Dembo, M., Drapeau, M., Elliott, M.C., Feuerriegel, E.M., Garcia-Martinez, D., Green, D.J., Gurtov, A., Irish, J.D., Kruger, A., Laird, M.F., Marchi, D., Meyer, M.R., Nalla, S., Negash, E.W., Orr, C.M., Radovcic, D., Schroeder, L., Scott, J.E., Throckmorton, Z., Tocheri, M.W., VanSickle, C., Walker, C.S., Wei, P., Zipfel, B., 2015. *Homo naledi*, a new species of the genus *Homo* from the Dinaledi Chamber, South Africa. Elife 4, e09560. https://doi.org/10.7554/eLife.09560.

Bookstein, F.L., Gunz, P., Mitteroecker, P., Prossinger, H., Schaefer, K., Sedler, H., 2003. Cranial integration in *Homo*: Singular warps analysis of the midsagittal plane in ontogeny and evolution. J. Hum. Evol. 44 (2), 167–187. https://doi.org/10.1016/S0047-2484(02)00201-4.

Brzobohatá, H., Prokop, J., Horák, M., Jančárek, A., Velemínská, J., 2012. Accuracy and benefits of 3D bone surface modelling: A comparison of two methods of surface data acquisition reconstructed by laser scanning and computed tomography outputs. Coll. Antropol. 3, 801–806.

Carretero, J.M., Quam, R.M., Gómez-Olivencia, A., Castilla, M., Rodríguez, L., García-González, R., 2015. The Magdalenian human remains from El Mirón Cave, Cantabria (Spain). J. Archaeol. Sci. 60, 10–27. https://doi.org/10.1016/j.jas.2015.03.026.

D'Angelo del Campo, M., Medialdea, L., García-Laborde, P., García-Martínez, D., Bastir, M., González-José, R., González-Martín, A., Guichón, R.A., 2023. Inter-method error in geometric morphometric and the relevance of texturization and landmark marking. Rev. Arg. Antrop. Biol. 25 (1), 1–18. https://doi.org/10.24215/18536387e057.

Engelkes, K., Helfsgott, J., Hammel, J.U., Büsse, S., Kleinteich, T., Beerlink, A., Gorb, A.B., Haas, A., 2019. Measurement error in μCT-based three-dimensional geometric morphometrics introduced by surface generation and landmark data acquisition. J. Anat. 235 (2), 357–378. https://doi.org/10.1111/joa.12999.

Fedorov, A., Beichel, R., Kalpathy-Cramer, J., Finet, J., Fillion-Robin, J.-C., Pujol, S., Bauer, C., Jennings, D., Fennessy, F., Sonka, M., Buatti, J., Aylward, S., Miller, J.V., Pieper, S., Kikinis, R., 2012. 3D slicer as an image computing platform for the quantitative imaging network. J. Magn. Reson. Imag. 30 (9), 1323–1341. https://doi.org/10.1016/j.mri.2012.05.001.

Feix, T., Kivell, T.L., Pouydebat, E., Dollar, A.M., 2015. Estimating thumb-index finger precision grip and manipulation potential in extant and fossil primates. J. R. Soc. Interface 12 (106), 20150176. https://doi.org/10.1098/rsif.2015.0176.

García-Martínez, D., Bastir, M., Riesco, A., 2018. Missing element estimation in sequential anatomical structures: The case of the human thoracic vertebrae and its potential application to the fossil record. In: Rissech, C., Lloveras, L., Nadal, J., Fullola, J.M. (Eds.), Geometric Morphometrics: Trends in Biology, Paleobiology and Archaeology. SERP, Barcelona, pp. 93–99.

Goodyear, M.D.E., Krleza-Jeric, K., Lemmens, T., 2007. The Declaration of Helsinki. Br. Med. J. 335 (7621), 624–625. https://doi.org/10.1136/bmj.39339.610000.BE.

Gunz, P., Mitteroecker, P., 2013. Semilandmarks: A method for quantifying curves and surfaces. Hystrix Ital. J. Mammal. 24 (1), 103–109. https://doi.org/10.4404/hystrix-24.1-6292.

Gunz, P., Mitteroecker, P., Bookstein, F.L., 2005. Semilandmarks in three dimensions. In: Slice, D. (Ed.), Modern Morphometrics in Physical Anthropology. Springer, New York, pp. 73–89.

Gunz, P., Mitteroecker, P., Neubauer, S., Weber, G.W., 2009. Principles for the virtual reconstruction of hominin crania. J. Hum. Evol. 57, 48–62. https://doi.org/10.1016/j.jhevol.2009.04.004.

Hall, B.K., 1992. Evolutionary Developmental Biology. Chapman & Hall, London.

Hall, B.K., 1995. Homology and embryonic development. In: Hecht, M.K., Macintyre, R.J., Clegg, M.T. (Eds.), Evolutionary Biology. Springer, Boston, pp. 1–37. https://doi.org/10.1007/978-1-4615-1847-1_1.

Hamrick, M.W., 2012. The developmental origins of mosaic evolution in the primate limb skeleton. Evol. Biol. 39, 447–455. https://doi.org/10.1007/s11692-011-9154-3.

Hunt, K.D., 2020. Chimpanzee: Lessons From our Sister Species. University Press, Cambridge.

Inouye, S.E., 1991. Ontogeny and allometry in African ape fingers. In: Ehara, E. (Ed.), Primatology Today. Elsevier, Tokyo, pp. 537–538.

Inouye, S.E., 1992. Ontogeny and allometry of African ape manual rays. J. Hum. Evol. 23 (2), 107–138. https://doi.org/10.1016/0047-2484(92)90103-G.

Inouye, S.E., 1994. Ontogeny of knuckle-walking hand postures in African apes. J. Hum. Evol. 26, 459–485. https://doi.org/10.1006/jhev.1994.1028.

Karakostis, F.A., Hotz, G., Tourloukis, V., Harvati, K., 2018. Evidence for precision grasping in Neanderthal daily activities. Sci. Adv. 4 (9), 1–11. https://doi.org/10.1126/sciadv.aat2369.

Kavanagh, K., 2020. Developmental plasticity associated with early structural integration and evolutionary patterns: Examples of developmental bias and developmental facilitation in the skeletal system. Evol. Dev. 22, 196–204. https://doi.org/10.1111/ede.12323.

Kavanagh, K.D., Shoval, O., Winslow, B.B., Alon, U., Leary, B.P., Kan, A., Clifford, J.T., 2013. Developmental bias in the evolution of phalanges. Proc. Natl. Acad. Sci. 45 (110), 18190–18195. https://doi.org/10.1073/pnas.1315213110.

Kivell, T.L., 2015. Evidence in hand: Recent discoveries and the early evolution of human hand manipulation. Phil. Trans. R. Soc. B 370 (1682), 20150105. https://doi.org/10.1098/rstb.2015.0105.

Kivell, T.L., Kibii, J.M., Churchill, S.E., Schmid, P., Berger, L.R., 2011. *Australopithecus sediba* hand demonstrates mosaic evolution of locomotor and manipulative abilities. Science 333 (9), 1411–1417. https://doi.org/10.1126/science.1202625.

Kivell, T.L., Deane, A.S., Tocheri, M.W., Orr, C.M., Schmid, P., Hawks, J., Berger, L.R., Churchill, S.E., 2015. The hand of *Homo naledi*. Nat. Commun. 6 (1), 1–9. https://doi.org/10.1038/ncomms9431.

Kivell, T.L., Churchill, S.E., Kiibi, J.M., Schmid, P., Berger, L.R., 2018. The hand of *Australopithecus sediba*. PaleoAnthropology 282–333.

Kivell, T.L., Baraki, N., Lockwood, V., Williams-Hatala, E.M., Wood, B.A., 2022. Form, function and evolution of the human hand. Yearb. Biol. Anthropol. 181 (76), 6–57. https://doi.org/10.1002/ajpa.24667.

Klingenberg, C.P., 2008. Morphological integration and developmental modularity. Annu. Rev. Ecol. Evol. Syst. 39, 115–132. https://doi.org/10.1146/annurev.ecolsys.37.091305.110054.

Kunze, J., Harvati, K., Hotz, G., Karakostis, A.F., 2024. Humanlike manual activities in Australopithecus. J. Hum. Evol. 196, 103591. https://doi.org/10.1016/j.jhevol.2024.103591.

Larson, S.G., Jungers, W.L., Tocheri, M.W., Orr, C.M., Morwood, M.J., Sutikna, T., Awe, R.D., Djubiantono, T., 2009. Descriptions of the upper limb skeleton of *Homo floresiensis*. J. Hum. Evol. 57, 555–570. https://doi.org/10.1016/j.jhevol.2008.06.007.

Lazenby, R.A., Skinner, M.M., Hublin, J.J., Boesch, C., 2011. Metacarpal trabecular architecture variation in the chimpanzee (*Pan troglodytes*): Evidence for locomotion and tool-use? Am. J. Phys. Anthropol. 144, 215–225. https://doi.org/10.1002/ajpa.21390.

Marchi, D., 2005. The cross/sectional geometry of the hand and foot bones of the Hominoidea and its relationship to locomotor behavior. J. Hum. Evol. 49, 743–761. https://doi.org/10.1016/j.jhevol.2005.08.002.

Mardia, K.V., Bookstein, F.L., Moreton, I.J., 2000. Statistical assessment of bilateral symmetry of shapes. Biometrika 87 (2), 285–300. https://doi.org/10.1093/biomet/87.2.285.

Marzke, M.W., 1997. Precision grips, hand morphology, and tools. Am. J. Phys. Anthropol. 102, 91–110. https://doi.org/10.1002/(SICI)1096-8644(199701)102:1%3C91::AID-AJPA8%3E3.0.CO;2-G.

Matarazzo, S.A., 2013. Knuckle-walking signal in the manual phalanges and metacarpals of the great apes (*Pan* and *Gorilla*). Ph.D. Thesis, University of Massachusetts, Amherst.

Matarazzo, S.A., 2015. Trabecular architecture of the manual elements reflects locomotor patterns in primates. PLoS One 10 (3), e0120463. https://doi.org/10.1371/journal.pone.0120436.

Mikkelsen, T.S., Hillier, L.W., Eichler, E.E., Zody, M.C., Jaffe, D.B., Yang, S.P., Enard, W., Hellmann, I., Lindblad-Toh, K., Altheide, T.K., Archidiacono, N., Bork, P., Butler, J., Chang, J.L., Cheng, Z., Chinwalla, A.T., de Jong, P., Delehaunty, K.D., Fronick, C.C., Fulton, L.L., Gilad, Y., Glusman, G., Gnerre, S., Graves, T.A., Hayakawa, T., Hayden, K.E., Huang, X., Ji, H., Kent, W.J., King, M.C., Kulbokas III, E.J., Lee, M.K., Liu, G., Lopez-Otin, C., Makova, K.D., Man, O., Mardis, E.R., Mauceli, E., Miner, T.L., Nash, W.E., Nelson, J.O., Pääbo, S., Patterson, N.J., Pohl, 2005. Initial sequence of the chimpanzee genome and comparison with the human genome. In: Pollard, K.S., Prüfer, K., Puente, X.S., Reich, D., Rocchi, M., Rosenbloom, K., Ruvolo, M., Richter, D.J., Schaffner, S.F., Smit, A.F.A., Smith, S.M., Suyama, M., Taylor, J., Torrents, D., Tuzun, E., Varki, A., Velasco, G., Ventura, M., Wallis, J.W., Wendl, M.C., Wilson, R.K., Lander, E.S., Waterston, R.H. (Eds.), Nature 437, 69–87. https://doi.org/10.1038/nature04072.

Mitteroecker, P., Gunz, P., 2009. Advances in geometric morphometrics. Evol. Biol. 36, 235–247. https://doi.org/10.1007/s11692-009-9055-x.

Musgrave, J.H., 1973. The phalanges of Neanderthal and Upper Palaeolithic hands. In: Day, M.H. (Ed.), Human Evolution. Taylor & Francis, London, pp. 59–85.

Napier, J.R., 1962. Fossil hand bones from Olduvai Gorge. Nature 196, 409–411. https://doi.org/10.1038/196409a0.

Niewoehner, W.A., 2006. Neanderthal hands in their proper perspective. In: Hublin, J.J., Harvati, K., Harrison, T. (Eds.), Neanderthals Revisited: New Approaches and Perspectives. Springer, Dordrecht, pp. 157–190. https://doi.org/10.1007/978-1-4020-5121-0_9.

Patel, B.A., Maiolino, S.A., 2016. Morphological diversity in the digital rays of primate hands. In: Kivell, T.L., Lemelin, P., Richmond, B.G., Schmitt, D. (Eds.), The Evolution of the Primate Hand. Springer, Berlin, pp. 55–100.

Pedersen, T., 2024. Patchwork: The composer of plots. R package version 1.3.0.9000. https://patchwork.data-imaginist.com.

Prabhakar, S., Visel, A., Akiyama, J.A., Shoukry, M., Lewis, K.D., Holt, A., Plajzer-Frick, I., Morrison, H., FitzPatrick, D.R., Afzal, V., Pennachio, L.A., Rubin, E.M., Noonan, J.P., 2008. Human-specific gain of function in a developmental enhancer. Science 321, 1346–1350. https://doi.org/10.1126/science.1159974.

R Core Team, 2023. R: A language and environment for statistical computing. R Foundation for Statistical Computing, Vienna, Austria.

Rasmussen, D.T., Tan, C.L., 1992. The allometry of behavioural development: Fitting sigmoid curves to ontogenetic data for use in interspecific allometric analyses. J. Hum. Evol. 23 (2), 159–181. https://doi.org/10.1016/0047-2484(92)90105-I.

Reno, P.L., McCollum, M.A., Cohn, M.J., Meindl, R.S., Hamrick, M., Lovejoy, C.O., 2008. Patterns of correlation and covariation of anthropoid distal forelimb segments correspond to Hoxd expression territories. J. Exp. Zool. B. 310B, 240–285. https://doi.org/10.1002/jez.b.21207.

Richmond, B.G., Green, D.J., Lague, M.R., Chirchir, H., Behrensmeyer, A.K., Bobe, R., Bamford, M.K., Griffin, N.L., Gunz, P., Mbua, E., Merritt, S.R., Pobiner, B., Kiura, P., Kibunjia, M., Harris, J.W.K., Braun, D.R., 2020. The upper limb of *Paranthropus boisei* from Ileret, Kenya. J. Hum. Evol. 141, 102727. https://doi.org/10.1016/j.jhevol.2019.102727.

Rolian, C., Lieberman, D.E., Hallgrímsson, B., 2010. The coevolution of human hands and feet. Evolution 64 (6), 1558–1568. https://doi.org/10.1111/j.1558-5646.2009.00944.x.

Rosas, A., Rodriguez-Perez, F.J., Bastir, M., Estalrrich, A., Huguet, R., García-Tabernero, A., Pastor, J.F., de la Rasilla, M., 2016. Adult Neandertal clavicles from the El Sidron site (Asturias, Spain) in the context of *Homo* pectoral girdle evolution. J. Hum. Evol. 95, 55–67. https://doi.org/10.1016/j.jhevol.2016.03.005.

Ross, A.H., Williams, S., 2008. Testing repeatability and error of coordinate landmark data acquired from crania. J. Forensic Sci. 53 (4), 782–785. https://doi.org/10.1111/j.1556-4029.2008.00751.x.

Schlager, S., 2017. Morpho and Rvcg – Shape analysis in R: R-packages for geometric morphometrics, shape analysis, and surface manipulations. In: Zheng, G., Li, S., Székely, G. (Eds.), Statistical Shape and Deformation Analysis. Academic Press, Cambridge, pp. 217–256.

Semal, P., Rougier, H., Crevecoeur, I., Jungels, C., Flas, D., Hauzeur, A., Maureille, B., Germonpré, M., Bocherens, H., Pirson, S., Cammaert, L., De Clerck, N., Hambucken, A., Highan, T., Toussaint, M., van der Plicht, J., 2009. New data on the late Neandertals: Direct dating of the Belgian Spy fossils. Am. J. Phys. Anthropol. 138, 421–428. https://doi.org/10.1002/ajpa.20954.

Shearer, B.M., Cooke, S., Halenar, L.B., Reber, S.L., Plummer, J.E., Delson, E., Tallman, M., 2017. Evaluating causes of error in landmark-based data collection using scanners. PLoS One 12 (11), 1–37. https://doi.org/10.1371/journal.pone.0187452.

Susman, R.L., 1979. Comparative and functional morphology of hominoid fingers. Am. J. Phys. Anthropol. 50, 215–236. https://doi.org/10.1002/ajpa.1330500211.

Susman, R.L., 1998. Hand function and tool behavior in early hominids. J. Hum. Evol. 35, 23–46. https://doi.org/10.1006/jhev.1998.0220.

Susman, R.L., Stern, J.T., Lungers, W.L., 1984. Arboreality and bipedality in the Hadar hominids. Folia Primatol. 43, 113–156. https://doi.org/10.1159/000156176.

Syeda, S.M., Tsegai, Z.J., Cazenave, M., Skinner, M.M., Kivell, T.L., 2023. Cortical bone distribution of the proximal phalanges in great apes: Implications for reconstructing manual behaviours. J. Anat. 243 (5), 707–728. https://doi.org/10.1111/joa.13918.

Syeda, S.M., Tsegai, Z.J., Cazenave, M., Skinner, M.M., Kivell, T.L., 2024. Cortical bone architecture of hominid intermediate phalanges reveals functional signals of locomotion and manipulation. Am. J. Biol. Anthropol. 184 (1), e24902. https://doi.org/10.1002/ajpa.24902.

Tocheri, M.W., Orr, C.M., Jakofsky, M.C., Marzke, M.W., 2008. The evolutionary history of the hominin hand since the last common ancestor of *Pan* and *Homo*. J. Anat. 212, 544–562. https://doi.org/10.1111/j.1469-7580.2008.00865.x.

Trinkaus, E., 1983. The Shanidar Neandertals. Academic Press, New York.

Trinkaus, E., 2016. The evolution of the hand in Pleistocene. In: Kivell, T.L., Lemelin, P., Richmond, B.G., Schmitt, D. (Eds.), The Evolution of the Primate Hand. Springer, Berlin, pp. 545–575.

Trinkaus, E., Maki, J., Zilhão, J., 2007. Middle Paleolithic human remains from the Gruta da Oliveira (Torres Novas), Portugal. Am. J. Phys. Anthropol. 134, 263–273. https://doi.org/10.1002/ajpa.20669.

Tsegai, Z.J., Kivell, T.L., Gross, T., Nguyen, N.H., Pahr, D.H., Smaers, J.B., Skinner, M.M., 2013. Trabecular bone structure correlates with hand posture and use in hominoids. PLoS One 8, e78781. https://doi.org/10.1371/journal.pone.0078781.

Wallace, I.J., Patel, B.A., 2013. Cross-sectional geometry of chimpanzee finger bones. Am. J. Phys. Anthropol. 150 (56), 283. https://doi.org/10.1096/fasebj.27.1_supplement.744.2.

White, T.D., 1980. Additional fossil hominids from Laetoli Tanzania: 1976-1979 specimens. Am. J. Phys. Anthropol. 53, 487–504. https://doi.org/10.1002/ajpa.1330530405.

Wickham, H., 2016. Ggplot2: Elegant Graphics for Data Analysis. Springer, New York.

Wickham, H., 2023. Stringr: Simple, consistent wrappers for common string operations. R package version 1.5.1. https://stringr.tidyverse.org.

Wickham, H., François, R., Henry, L., Müller, K., Vaughan, D., 2023. Dplyr: A grammar of data manipulation. R package version 1.1.4. https://stringr.tidyverse.org.

Wickham, H., Vaughan, D., Girlich, M., Ushey, K., 2024. Tidyr: Tidy messy data. R package version 1.3.1. https://tidyr.tidyverse.org.

Zelditch, M.L., Swiderski, D.L., Sheets, H.D., Fink, W.L., 2012. Geometric Morphometrics for Biologists: A Primer. Academic Press, San Diego.